# Changes in protein conformational mobility upon activation of extracellular regulated protein kinase-2 as detected by hydrogen exchange

**Andrew N. Hoofnagle*, Katheryn A. Resing*, Elizabeth J. Goldsmith†, and Natalie G. Ahn*‡§**

*Department of Chemistry and Biochemistry, and ‡Howard Hughes Medical Institute, University of Colorado, Boulder, CO 80309; and †Department of Biochemistry, University of Texas Southwestern Medical Center, Dallas, TX 75235

Communicated by Judith P. Klinman, University of California, Berkeley, CA, November 27, 2000 (received for review September 18, 2000)

**Changes in protein mobility accompany changes in conformation during the trans-activation of enzymes; however, few studies exist that validate or characterize this behavior. In this study, amide hydrogen/deuterium exchange/mass spectrometry was used to probe the conformational flexibility of extracellular signal-regulated protein kinase-2 before and after activation by phosphorylation. The exchange data indicated that extracellular regulated protein kinase-2 activation caused altered backbone flexibility in addition to the conformational changes previously established by x-ray crystallography. The changes in flexibility occurred in regions involved in substrate binding and turnover, suggesting their importance in enzyme regulation.**

The mitogen-activated protein (MAP) kinase extracellular regulated protein kinase-2 (ERK2) plays a central role in signaling pathways regulating cell growth and differentiation in eukaryotic cells. Phosphorylation at Thr-183 or Tyr-185 by MAP kinase (MAPK) kinase-1/2 leads to >1,000-fold enhanced specific kinase activity, resulting in elevated phosphorylation of cellular targets including transcription factors and downstream kinases (1). ERK2 presents an attractive model system for understanding regulated changes involved in enzyme activation, because x-ray structures are available for both inactive, unphosphorylated (ERK) and active diphosphorylated (ppERK) kinases (2, 3).

X-ray structures of ERK2 show features conserved in protein kinase catalytic cores (2, 4) (Fig. 1*b*). These include the N-terminal lobe ($\beta$1–$\beta$5 and helix $\alpha$C) and the larger C-terminal lobe (helices $\alpha$D–$\alpha$I and $\beta$6–$\beta$9), which are responsible for nucleotide and protein substrate binding, respectively, and which surround residues in the catalytic cleft that facilitate phosphoryl transfer. A hinge joins the two lobes and serves as the pivot for domain closure, a conformational change associated with formation of the ternary enzyme-substrate complex (5). The phosphorylation sites in ERK2 are contained in the activation lip, a key site for regulatory phosphorylation and substrate recognition in protein kinases (4, 6).

Phosphorylation causes major rearrangements within the activation lip and the adjacent P + 1 protein substrate specificity site (3, 7) (Fig. 1*a*). These structural rearrangements create a competent substrate binding pocket and properly orient residues necessary for phosphoryl transfer. In addition, phosphorylation induces structural changes in a C-terminal extension (L16), forming a homodimerization interface and stable dimers in active ppERK, but not in inactive ERK (8) (Fig. 1 *b* and *c*). Minor structural changes also occur within the MAPK insert ($\alpha$1L14 and $\alpha$2L14) where side-chain interactions with the activation lip are disrupted (Fig. 1 *b* and *c*).

Limited information is available on kinase flexibility and dynamics, factors that are presumably critical to the regulation of enzyme activity. Advances in hydrogen exchange/mass spectrometry (HX/MS) enable analysis of solution conformational ensembles for larger proteins such as protein kinases (9–11). By measuring exchange between protein backbone amide hydrogens and deuterated water, HX measurements report chemical environment and secondary structure, because exchange rates are reduced by hydrogen bonding and/or burial within the protein (12–16). In addition, theory predicts that observed rates are proportional to the equilibrium constants for conversion between solvent accessible and inaccessible conformations (17–20). HX measurements report internal motions of the folded state because exchange at neutral pH under nondenaturing conditions predominantly occurs through low energy fluctuations in protein structure that enable transient solvent accessibility.

In this study, changes in HX rate in peptides derived from intact, labeled ERK and ppERK were monitored by HX/MS, and these changes were compared with conformational changes in corresponding regions of the x-ray structures. In the activation lip and dimerization interface, HX rates increased or decreased in a manner that coincided with changes in conformation, assessed by the number of amide hydrogen bonds and the degree of amide hydrogen burial. In contrast, in the ATP binding loop, hinge, and substrate binding site, changes in HX rates occurred in a manner unaccountable by x-ray structures, but consistent with changes in backbone flexibility upon activation. These results illustrate the power of HX/MS to complement static structural information from x-ray crystallography by providing insight into internal motions of enzymes. Importantly, we demonstrate that kinase activation by phosphorylation not only leads to changes in conformation, but also causes significant changes in protein mobility in regions important for catalysis.

## Methods

**HX Measurements.** $(His)_6$-tagged rat ERK2 was expressed in *Escherichia coli* and stoichiometrically diphosphorylated with the constitutively active mutant MAPK kinase-1 G7B (MKK1-G7B), and both ERK and ppERK were further purified by FPLC and stored in aliquots at −80°C as described (1, 16, 21). The HX experiments were performed as described, using separate aliquots of enzyme for each measurement within 3 h after thawing, and alternating measurements of ERK and ppERK (16). Exchange reactions were performed from 7 sec to 5 h by using 5 $\mu$g (50 $\mu$g/ml) of kinase in 90% $D_2O$, 2.5 mM $KPO_4$ (pH 7.4), 12.5 mM KCl, and 0.25 mM DTT at 10°C. Reactions were quenched by acidification and cooling, digested with pepsin, and analyzed on a reversed-phase capillary column (POROS R120, PerSeptive

Abbreviations: ERK2, extracellular regulated protein kinase-2; ERK, unphosphorylated/inactive ERK2; ppERK, diphosphorylated/active ERK2; HX/MS, hydrogen exchange/mass spectrometry; MAP, mitogen-activated protein; MAPK, MAP kinase.

§To whom reprint requests should be addressed at: Department of Chemistry and Biochemistry, Howard Hughes Medical Institute, Campus Box 215, University of Colorado, Boulder, CO 80309. E-mail: ahnn@spot.colorado.edu.

The publication costs of this article were defrayed in part by page charge payment. This article must therefore be hereby marked "*advertisement*" in accordance with 18 U.S.C. §1734 solely to indicate this fact.

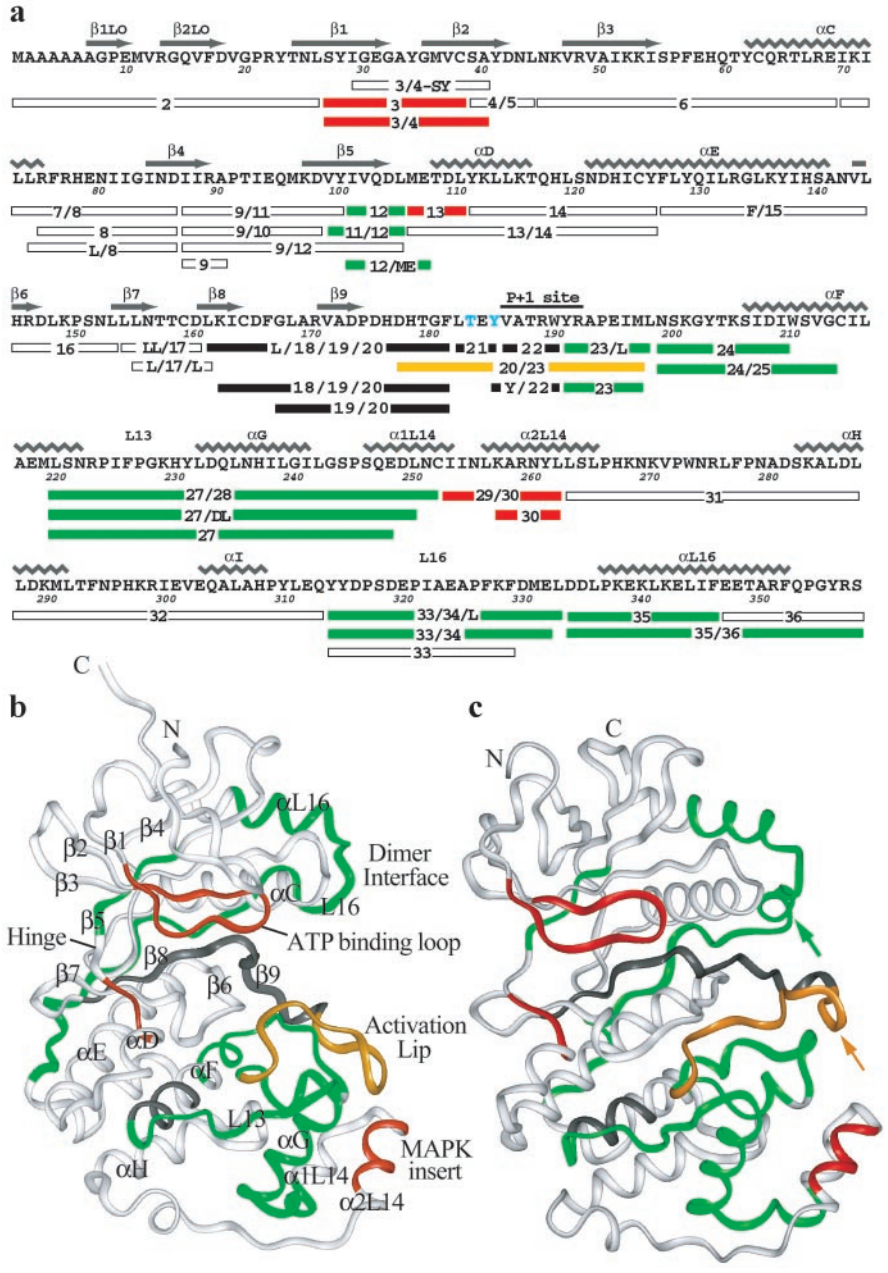


**Fig. 1.** Peptides analyzed in this study. (*a*) Sequence coverage of ERK2 indicating residue numbering and secondary structure as in Zhang *et al.* (2). Peptides colored red, green, yellow, or white showed HX rates that, respectively, increased, decreased, both increased and decreased, or did not change upon kinase phosphorylation. Peptides recovered only from unphosphorylated ERK but not ppERK are shown in black. Residues phosphorylated in ppERK are shown in blue. (*b*) Structural representation of ERK (2). Sequences not recovered from peptide digests are colored gray. (*c*) Structural representation of ppERK (3) as in *b*, rotated slightly clockwise (as viewed down the vertical axis) to more clearly show the major differences with the inactive form, the reorganization of the activation lip (yellow arrow) and the formation of a 3/10-helix near the C terminus (green arrow).

Biosystems, Framingham, MA) coupled to an API-III$^+$ triple quadrupole mass spectrometer (Perkin–Elmer Biosystems). The time from the initiation of digestion to the elution of all peptides was 22 min. Zero time point controls were performed by adding quench buffer before $D_2O$.

Measured peptide masses were corrected for exchange at $t = 0$, normalized to 100% $D_2O$, and corrected for back-exchange as described (16). Kinetics of exchange using corrected peptide masses were fit by nonlinear least squares to the equation: $Y = N - Ae\text{-}k^1t - Be\text{-}k^2t - Ce\text{-}k^3t$ (DATAFIT 6.1, Oakdale Engineering, Oakdale, PA), where $N$ is the peptide mass after complete exchange of deuterium at backbone amides, and $A$, $B$, and $C$ correspond to the number of amides exchanging with rate constants $k_1$, $k_2$, and $k_3$, respectively (16). In the text, $A$, $B$, $C$, and $N$ are reported to the nearest integer.

**Calculation of Hydrogen Bond Length and Distance-to-Surface for Amide Hydrogens.** X-ray coordinates of monomeric ERK and monomeric ppERK were as described [Protein DataBank codes 1ERK (2) and 2ERK (3)]. Neither structure contains ATP, although subsequent diffusion into the crystal demonstrates interaction of the adenine ring with the backbone of residues Asp-104 and Met-106 (2, 22). Coordinates of the second monomer in dimeric ppERK were obtained from the crystallographic

symmetry (3). Amide hydrogens were positioned in the x-ray structure, and hydrogen bonds were identified by using INSIGHTII, constraining donor (D) to acceptor (A) distances <3.0 Å, and D-H-A and C-A-H angles >90° (16). The shortest distance between each amide hydrogen and the surface was calculated by using the program MINSURF (written by Leland Mayne, Univ. of Pennsylvania, Philadelphia, and provided by John Milne and S. Walter Englander, Univ. of Pennsylvania, Philadelphia), which uses a molecular surface calculated with the Connolly algorithm and a probe radius of 1.4 Å (15). Back-exchange calculations were performed by using HXPEP, written and provided by Zhongqi Zhang (Amgen, Thousand Oaks, CA), based on an algorithm described in ref. 23. Figs. 2*d* and 3*f* were generated by using MOLSCRIPT 1.4 (24) and RASTER-3D (25).

## Results

**HX Rate Measurements.** HX exchange rates for ERK vs. ppERK were measured by incubating proteins for varying times in $D_2O$, in the absence of ATP or protein substrate. After quenching the exchange, protein was digested by limited proteolysis, and masses of the resulting peptides were determined by liquid chromatography/MS (LC/MS). This measures deuteration at backbone amides, because side-chain deuterons back-exchange to hydrogen during LC/MS. Thirty-nine peptides were sequenced by MS, which provided 90% coverage (330 of 366 amides) over the entire backbone (Fig. 1*a*). Kinetics of exchange for each peptide were fit by a nonlinear least-squares method to sums of exponentials (e.g., Figs. 2 and 3). This yielded exchange rates ranging between 0.002 $min^{-1}$ and >14 $min^{-1}$ in 56% of observed amides (see Table 1, which is published as supplemental data on the PNAS web site, www.pnas.org); for convenience, these rates were classified as fast (>1.0 $min^{-1}$), intermediate (0.1–1.0 $min^{-1}$), or slow (0.002–0.1 $min^{-1}$). The remaining 44% of amides showed no exchange within 5 h (<0.002 $min^{-1}$, nonexchanging). The back-exchange during the experiment averaged over all peptides was 22 ± 6%, consistent with the calculated value of 23% for peptides in low salt at 0°C (23).

Twenty of the 39 peptides (some overlapping) showed differences upon ERK2 activation, including five peptides with increased exchange rates (Fig. 1, indicated in red), 14 peptides with decreased rates (Fig. 1, indicated in green), and one that showed complex behavior reflecting both increased and decreased rates (Fig. 1, indicated in yellow). Peptides displaying the greatest changes were from regions known to be involved in substrate binding and catalysis, with minor deviations in the MAPK insert. Differences also were observed in and near the C-terminal extension, a crystal contact shown by mutagenesis to function as an interface for homodimerization.

**HX Rates Reporting Changes in Conformation.** To interpret the x-ray structure in terms of solvent accessibility of amides and hydrogen bonding, atomic coordinates of monomeric ERK and dimeric ppERK were used to calculate the positions of the amide hydrogens, the distance of each amide to the solvent accessible surface (distance-to-surface), and the length and orientation of amide hydrogen bonds (2, 3, 15). Regions of altered exchange were analyzed in terms of changes in both distance-to-surface and the number of hydrogen bonds, which modulate exchange rates through changes in steric protection and altered reactivity to proton abstraction. For example, peptides 35 and 33/34/L, which encompass the dimer interface in ppERK (8) (Fig. 1 *a* and *b*), both showed decreased rates consistent with changes in solvent protection (Fig. 2*a*). A 2-fold decrease in rate of the slow class was measured for peptide 35, consistent with the significant reduction in solvent accessibility in this region, particularly at amide 335 (Fig. 2*b*). In addition, peptide 33/34/L showed a 2-fold decrease in the intermediate rate class, concomitant with new hydrogen bonds established due to reorganization of L16

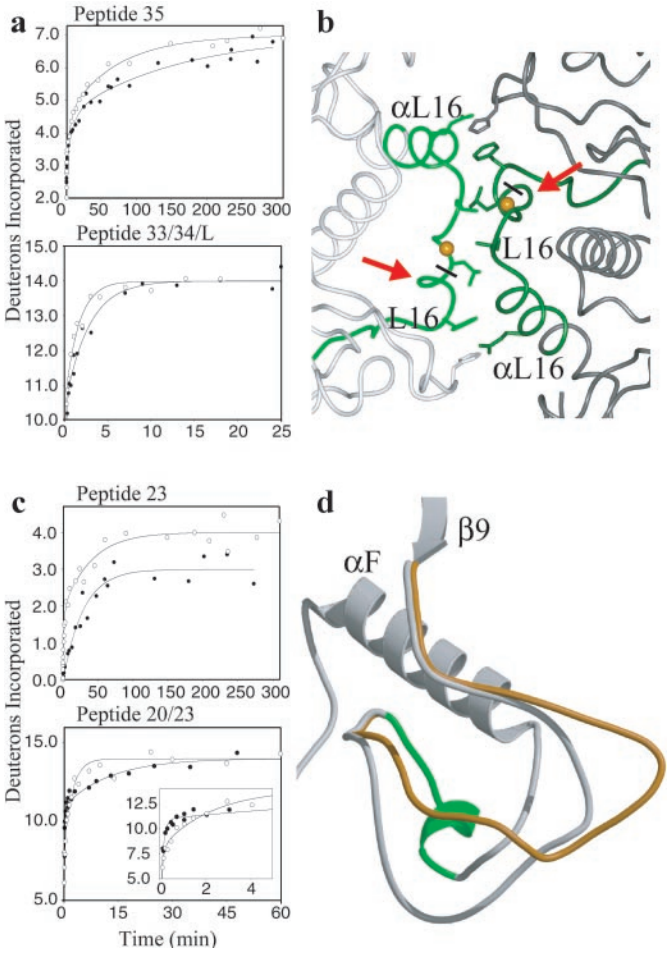


**Fig. 2.** Comparison of peptide HX kinetics and associated x-ray structural changes in ERK (○) and ppERK (●) in the dimer interface and activation lip. (*a*) Deuterons incorporated vs. time is shown for peptides 35 and 33/34/L in the dimer interface. Exchange into peptide 35 in 5 h totaled seven of 11 amides, and curve fitting indicated a decreased rate upon ERK activation of two amides from $k_{3(ERK)} = 0.014\ min^{-1}$ to $k_{3(ppERK)} = 0.006\ min^{-1}$. In peptide 33/34/L, 14 of 16 amides exchanged, with decreased rate for the slow class (four amides; $k_{2(ERK)} = 0.64\ min^{-1}$; $k_{2(ppERK)} = 0.37\ min^{-1}$). (*b*) X-ray structure of the dimer interface illustrating the phosphorylation induced 3/10 helix (arrow) and side-chain associations that contribute to dimer formation. Amide hydrogens of Asp-335 from each monomer are represented by orange spheres and the cleavages between peptides 35 and 33/34/L by black bars. (*c*) Kinetics of exchange for activation lip peptides 23 and 20/23 as in *a*. In peptide 23, four of five amides exchanged in ERK and three exchanged in ppERK. In the simplest model, ERK activation led to a 1.8-fold decrease in rate for the intermediate class (two amides; $k_{2(ERK)} = 0.62\ min^{-1}$; $k_{2(ppERK)} = 0.35\ min^{-1}$) and a conversion of one slow amide to nonexchanging. Peptide 20/23 has 19 amides of which 14 exchange. Phosphorylation led to complex effects involving both a decrease at short times (*Inset*) and an increase at longer times. (*d*) Ribbon diagram illustrating structural changes in the activation lip. The conformation of peptide 23 and residues 177–190 of peptide 20/23 in ppERK are shown in green and orange, respectively. Corresponding residues 177–190 in ERK are shown in gray.

from coil to 3/10 helix. These results further validate the existence in solution of the crystallographically observed dimer interface.

The HX rate behavior also agreed with structural changes at the activation lip. The total exchange in this region was significantly greater than the average over the rest of the molecule, consistent with its high solvent accessibility in the x-ray structure. Altered proteolytic cleavage occurred at Thr-183 and Tyr-185 after phosphorylation, which complicated comparison between

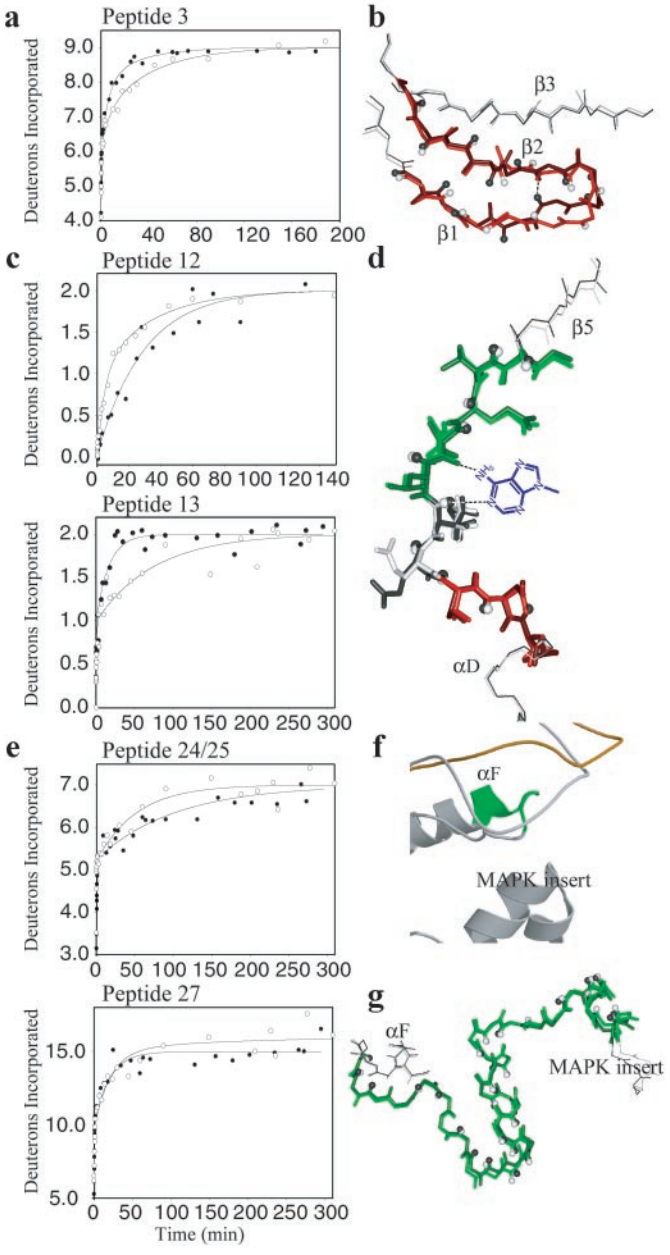


**Fig. 3.** Comparison of HX/MS data and x-ray structure in the ATP binding loop, hinge, and the extended peptide substrate binding groove. (*a*) Peptide 3 in the ATP binding loop has 11 amides of which nine exchange, where the increased exchange in ppERK indicates conversion of one slow amide to an intermediate amide ($k_{3(ERK)}$ = 0.024 min$^{-1}$; $k_{2(ppERK)}$ = 0.16 min$^{-1}$). (*b*) Conformational change in peptide 3 for ERK (white, red) and ppERK (gray, dark red), representing amide hydrogens by spheres and the backbone hydrogen bond formed between residues 32 and 35 in ppERK as a dotted line. (*c*) The hinge peptides 12 and 13 each showed two of four amides exchanging. In peptide 12, the decreased rate is consistent with conversion of one intermediate amide to a slow amide ($k_{2(ERK)}$ = 0.21 min$^{-1}$; $k_{3(ppERK)}$ = 0.035 min$^{-1}$), whereas in peptide 13 one slow amide increased in rate ($k_{3(ERK)}$ = 0.013 min$^{-1}$; $k_{3(ppERK)}$ = 0.060 min$^{-1}$). Decreased exchange in overlapping peptide 12/ME (not shown) was identical to the decreased exchange in peptide 12, indicating that no change in rate occurred at residues Met-106 and Glu-107, within peptides 12/ME and 13. (*d*) Superposition of the hinge ($rmsd_{backbone}$ = 0.33 Å) as in *b*, showing peptide 12 in green and peptide 13 (excluding Met-106 and Glu-107) in red. Shown in blue is the adenine ring of ATP, which if present would directly contact peptide 12 (28). (*e*) Peptides 24 and 27 in the extended substrate binding groove. Peptide 24 shows seven of 10 amides exchanging, best fit to decreased rates for both the fast amides (five amides; $k_{1(ERK)}$ = 11 min$^{-1}$; $k_{1(ppERK)}$ = 3.3 min$^{-1}$) and the slow amides (two amides; $k_{3(ERK)}$ = 0.019 min$^{-1}$; $k_{3(ppERK)}$ = 0.010 min$^{-1}$). Peptide 27 shows 17 of 25 amides exchanging, fit to the conversion of one slow amide (0.002 min$^{-1}$) to nonexchanging. (*f*) Ribbon diagram of the substrate binding groove, indicating peptide 24 in green (format as in Fig. 2*d*). (*g*) Superposition of peptide 27 of ERK (green) and ppERK (dark green) with $rmsd_{backbone}$ = 0.50 Å (format as in *b*).

ERK and ppERK within residues 162–177 (Fig. 1*a*). Where comparable peptides were generated, the observed changes in HX were consistent with the x-ray structure. One of these, peptide 23 (residues 191–197), encompasses a 3/10 helix at the C terminus of the activation lip, where three amides were buried upon phosphorylation. These included the amide hydrogen at Ala-193, whose distance-to-surface increased by >5 Å, the greatest increase in solvent protection between the two structures (Fig. 2*d*). Accordingly, peptide 23 showed the greatest decrease in total exchange after 5 h (Fig. 2*c*), with the best-fit model predicting conversion of one slow amide to nonexchanging and two intermediate amides to slow. In addition, peptide 20/23 (residues 178–197), containing the phosphorylation sites and the P + 1 substrate binding loop, showed complex behavior indicating both increased and decreased exchange rates due to interconversion between fast, intermediate, and slow classes (Fig. 2*c*). In the x-ray structures, one hydrogen bond was broken (amide 179) and three new hydrogen bonds were formed (amides 180, 181, and 183) upon phosphorylation, whereas amides 187 and 181 became buried and unburied, respectively. Although the complexity in this region precluded precise interpretation of exchange rate interconversions, overall the data reflected both increased and decreased solvent exposure predicted by the x-ray structures.

**HX Rates Reporting Regulation of Protein Mobility.** Four regions in ERK2 showed altered HX behavior upon activation that were inconsistent with the conformational changes demonstrated by crystallography. These were the glycine-rich ATP binding loop, the hinge region, the extended substrate binding groove, and the MAPK insert. In the first three, changes in protein flexibility occurred within regions of the molecule that are distant from the site of phosphorylation and are known to be important for substrate binding and catalysis (1, 2, 4–8, 22).

The first case is peptide 3, which contains the glycine-rich loop between $\beta$1 and $\beta$2, a key site for contact with the nucleotide triphosphate (4). The least-squares fit for peptide 3 indicated a 7-fold rate increase of one slow amide in ERK to an intermediate amide in ppERK (Fig. 3*a*). However, the ppERK structure predicts reduced exchange in this region, with a new hydrogen bond at amide 32 and a marked decrease in *B* factors (from 70 to 15 Å$^2$) ascribed in part to side-chain interactions between Tyr-34 and Tyr-62 in helix $\alpha$C (3) (Fig. 3*b*). The discordant behavior between the HX/MS measurements and x-ray conformation reveals increased protein mobility in this region upon ERK2 activation, although differences between solution and crystal structures cannot be ruled out. Enhanced flexibility in this region may contribute to catalysis in ppERK by facilitating ATP binding and/or ADP release. The importance of the ATP binding loop to catalysis is supported by the variable conformations observed in different cocrystal structures of protein kinase A with ATP, ADP, and adenosine, leading to the proposal that gating movements of the loop are critical for nucleotide association and dissociation (26, 27).

Peptides 12 and 13 comprise the hinge of ERK2, the second region that apparently undergoes a change in flexibility upon activation. The hinge backbone includes the pivot for opening and closing the active site cleft (26, 28) and sites of contact for the adenosine ring of ATP (2, 22). Exchange data for peptide 12

fit to a 6-fold decrease in the intermediate rate upon ERK phosphorylation. In contrast, data for peptide 13 fit to a 4-fold increase in the slow rate (Fig. 3*c*). However, none of the backbone amides in either peptide 12 or 13 showed any changes in distance-to-surface or number of hydrogen bonds between the two structures, which were nearly superimposable in this region (Fig. 3*d*). Thus the change in HX behavior most likely reflects alterations in backbone flexibility, in which the magnitude of the difference in $\Delta G_{HX}$ for the conversion between solvent accessible and inaccessible conformations is a function of observed HX rate constants [$\Delta\Delta G_{HX} = -RT\ln(k_{obs,ppERK}/k_{obs,ERK})$] (20). The calculated $\Delta\Delta G_{HX}$ is $\pm$0.8–1.0 kcal/mol, which is consistent with the energetics of conformational fluctuations of the folded state (20). We hypothesize that the region corresponding to peptide 12, which has been shown to form hydrogen bonds with the adenosine ring of ATP (2, 22), adopts a more rigid structure before nucleotide binding thus reducing the entropic cost of association. We also envision that increased motions in the region corresponding to peptide 13, which includes the N terminus of $\alpha$D, likely contributes to enhanced flexibility vital for domain closure during catalysis.

Residues 199–248 spanning helices $\alpha$F, $\alpha$G, and the intervening L13 loop comprise the third region in which HX/MS indicates a change flexibility. Exchange data for overlapping peptides 24 (residues 199–209) and 24/25 (residues 199–213) fit within error to identical decreases in both fast and slow rate classes, which were therefore localized to peptide 24 (Fig. 3*f*). These decreases were inconsistent with the structure of residues 200–205, where amide hydrogens are highly solvent exposed in ppERK vs. ERK, with an average decrease in distance-to-surface of 1.7 Å (Fig. 3*g*). Likewise, peptide 27 (residues 220–248) and overlapping peptides 27/DL and 27/28 all fit to the conversion of one slow amide to a nonexchanging amide, whereas x-ray structural comparison showed no changes in hydrogen bonding or distance-to-surface (Fig. 3 *f* and *h*). This region forms an extended peptide substrate binding groove (3) in protein kinase A (29) and twitchin (30) and also corresponds to the c-Jun D-domain binding site in c-Jun N-terminal protein kinase (31). It is therefore likely to form at least part of the protein substrate binding site in ERK2. The HX/MS measurements clearly indicate decreased conformational mobility in this region upon activation, which likely functions to promote protein substrate binding, thus contributing to enzymatic turnover.

The last region of altered deuterium exchange is peptide 30, spanning residues 256–262 of the MAPK insert. The HX/MS data fit to an increase of one nonexchanging amide converting to a slow amide (0.002 $min^{-1}$) upon ERK phosphorylation (data not shown). Structural contacts between the side chains in the insert (Ile-254) and the activation lip (Phe-181 and Leu-182) are disrupted after reorganization of the activation lip (3). However, this led to no change in hydrogen bonding or distance-to-surface of the backbone amide hydrogens, although the *B* factors increased from 10 to 50 $Å^2$. Thus, in the context of little structural change, the increased exchange rates in peptide 30 revealed enhanced conformational mobility in the MAPK insert.

## Discussion

By comparing the HX solution behavior of ERK2 to the structural information available from x-ray crystallography, we demonstrate that phosphorylation and activation of this enzyme leads to significant changes in its flexibility. There is surprisingly little experimental evidence for the common expectation that enzyme mobility influences catalysis (32, 33), particularly with larger enzymes like protein kinases. Our study correlates changes in internal motions with enzyme activation and shows that such changes occur in localized regions of the protein.

HX/MS of ERK2, measured in solution at physiological concentrations, confirmed that conformational changes occurred in the homodimerization interface and the activation lip after phosphorylation, as predicted from x-ray studies. In contrast, altered HX occurred in other regions in a manner inconsistent with the x-ray structure, and were thus more likely explained by altered protein mobility. Three of these regions are known to contribute to catalysis. First, the ATP binding loop showed an enhanced exchange rate inconsistent with the x-ray structure, thus indicating enhanced flexibility of this region upon activation. In protein kinase A, which is constitutively active in the absence of its regulatory subunit, flexibility of the corresponding loop has been postulated to permit the rate-limiting release of ADP (26–28). In ERK2, enhanced flexibility in the phosphate binding loop also may contribute to increased specific activity by facilitating nucleotide binding or release. Second, the hinge in ERK2 showed decreased exchange rate within the ATP binding site and increased exchange at the N terminus of $\alpha$D in the absence of any x-ray structural change. In protein kinases the hinge is critical for domain closure and formation of the active site cleft, as well as for binding the adenine ring of ATP (2, 22, 26, 28). Enhanced flexibility in $\alpha$D may facilitate domain closure vital for enzyme activity, whereas decreased flexibility in $\beta$5 may favor subsequent ATP binding. Third, two peptides in ERK2 that show decreased exchange encompass the extended peptide substrate binding groove (6). One showed decreased exchange in the absence of any x-ray structural change, whereas the other showed decreased exchange despite markedly decreased distance-to-surface in the x-ray structure. It is significant that those regions of ERK2 that become more solvent accessible upon phosphorylation, in a manner ascribed to enhanced flexibility, are those that are thought to move in the catalytic mechanism and are thus likely to contribute to enzyme activation. Conversely those regions that become less solvent accessible upon phosphorylation are those thought to be involved in substrate binding. Decreased flexibility in these regions could contribute to kinase activation by reducing the entropic cost of substrate binding.

Kinetic studies show that the major effect of phosphorylation and activation of ERK2 is to increase $k_{cat}$ by 50,000-fold, with minor effects on the binding affinity for ATP and peptide substrate (34). It is therefore conceivable that the changes in mobility in ERK2 that we observe are important for enhancing the rate of phosphoryl transfer. Two other examples exist in which changes in protein dynamics can be correlated with changes in the rate of the chemical step. First, studies by Klinman and colleagues (35) on glucose oxidase show that reducing protein flexibility by glycosylation correlates with a reduced degree of hydrogen tunneling in the hydrogen transfer step of the enzymatic reaction (35). Because hydrogen tunneling depends on vibrational modes of donor and acceptor atoms, this implies that the protein flexibility can be transmitted to the vibrational modes of bound substrates. Second, in studies by Imoto and colleagues (36), deletion of Arg-14 and His-15 at $\geq$ 20 Å from the catalytic center of lysozyme leads to a 1.4-fold increase in chitinase activity (36). Recently, NMR relaxation measurements showed that this mutation altered $^{15}$N-relaxation rates of several residues at or near the active site (37). These studies offer correlative but compelling evidence for the contribution of protein dynamics to enzyme catalysis.

What are the amplitudes and time scales of the motions in enzymes that are needed to facilitate catalysis? In the two-state Linderstrøm–Lang model, HX rates report the equilibrium between open and closed native-state conformations, thus changes in exchange rates reflect changes in kinetics of opening and closing. It currently is thought that micro to millisecond time-scale fluctuations are most relevant to HX behavior, although there is no theoretical basis to exclude the importance of shorter time-scale motions on the exchange process (17–20). We therefore can estimate only an upper limit of milliseconds for the

motions that affect HX, which nevertheless includes loop movements, fluctuations in domain orientation, and other motions that are very likely to be important in substrate turnover. On the other hand, an equally valid interpretation is to view changes in equilibria as being due to changes in the number of conformational states in the ground-state ensemble, and thus the probability of exchange from the subset of open conformations (13). This would predict a change in average conformation upon ERK2 phosphorylation. We observed minimal differences between ERK2 and ppERK2 in crystallographic structure in the glycine-rich loop, hinge, and extended peptide substrate binding groove, thus to the extent that x-ray structures reflect an average of native-state conformations, we would conclude that the number of conformers is not altered in the phosphorylated ERK2 ensemble. However, x-ray structures may in fact represent one of the many energetically favorable conformations visited in solution. Therefore kinetic vs. statistical mechanical interpretations of the deuterium exchange data cannot be distinguished, and both deserve consideration. As a better theoretical understanding of the motions and time scales important in HX unfolds, these methods should provide a wealth of information on mechanisms by which protein motions control catalysis.

We are indebted to Nick Tolwinski for assistance with data analysis. Special thanks to Arthur Pardi and Tonny DeBeer for many helpful discussions and critical reading of the manuscript. Financial support for this work was provided by National Institutes of Health Grant GM48521 (to N.G.A.). A.N.H. was funded by National Institutes of Health Medical Scientist Training Program Training Grant GM08497. K.A.R. recognizes funding from the National Institutes of Health (Grant AR43768), and E.J.G. recognizes funding from the National Institutes of Health (Grant DK46993) and the Welch Foundation (Grant I1128).

1. Robbins, D. J., Zhen, E., Owaki, H., Vanderbilt, C. A., Ebert, D., Geppert, T. D. & Cobb, M. H. (1993) *J. Biol. Chem.* **268,** 5097–5106.
2. Zhang, F., Strand, A., Robbins, D., Cobb, M. H. & Goldsmith, E. J. (1994) *Nature (London)* **367,** 704–711.
3. Canagarajah, B. J., Khokhlatchev, A., Cobb, M. H. & Goldsmith, E. J. (1997) *Cell* **90,** 859–869.
4. Taylor, S. S. & Radzio-Andzelm, E. (1994) *Structure (London)* **2,** 345–355.
5. Cox., S., Radzio-Andzelm, E. & Taylor, S. S. (1994) *Curr. Opin. Struct. Biol.* **4,** 893–901.
6. Johnson, L. N., Noble, M. E. M. & Owen, D. J. (1996) *Cell* **85,** 149–158.
7. Goldsmith, E. J. & Cobb, M. H. (1994) *Curr. Opin. Struct. Biol.* **4,** 833–840.
8. Khokhlatchev, A. V., Canagarajah, B., Wilsbacher, J., Robinson, M., Atkinson, M., Goldsmith, E. & Cobb, M. H. (1998) *Cell* **93,** 605–615.
9. Johnson, R. S. & Walsh, K. A. (1994) *Protein Sci.* **3,** 2411–2418.
10. Zhang, Z., Post, C. B. & Smith, D. L. (1996) *Biochemistry* **35,** 779–791.
11. Resing, K. A. & Ahn, N. G. (1998) *Biochemistry* **37,** 463–475.
12. Pedersen, T. G., Sigurskjold, B. W., Andersen, K. V., Kjœr, M., Poulsen, F. M., Dobson, C. M. & Redfield, C. (1991) *J. Mol. Biol.* **218,** 413–426.
13. Hilser, V. J. & Friere, E. (1996) *J. Mol. Biol.* **262,** 756–772.
14. Mori, S., Abeygunawardana, C., Berg, J. M. & van Zijl, P. C. M. (1997) *J. Am. Chem. Soc.* **119,** 6844–6852.
15. Milne, J. S., Roder, M. H., Wand, A. J. & Englander, S. W. (1998) *Protein Sci.* **7,** 739–745.
16. Resing, K. A., Hoofnagle, A. N. & Ahn, N. G. (1999) *J. Am. Soc. Mass Spectrom.* **10,** 685–702.
17. Bai, Y., Englander, J. J., Mayne, L., Milne, J. S. & Englander, S. W. (1995) *Methods Enzymol.* **259,** 344–356.
18. Miller, D. W. & Dill, K. A. (1995) *Protein Sci.* **4,** 1860–1873.
19. Clarke, J. & Itzhaki, L. S. (1998) *Curr. Opin. Struct. Biol.* **8,** 112–118.
20. Li, R. & Woodward, C. (1999) *Protein Sci.* **8,** 1571–1591.
21. Shapiro, P. S., Whalen, A. M., Tolwinski, N. S., Wilsbacher, J., Froelich-Ammon S. J., Garcia, M., Osheroff, N. & Ahn, N. G. (1999) *Mol. Cell. Biol.* **19,** 3551–3560.
22. Fox, T., Coll, J. T., Xie, X., Ford, P. J., Germann, U. A., Porter, M. D., Pazhanisamy, S., Fleming, M. A., Galullo, V., Su, M. S. & Wilson, K. P. (1998) *Protein Sci.* **7,** 2249–2255.
23. Bai, Y., Milne, J. S., Mayne, L. & Englander, S. W. (1993) *Proteins* **17,** 75–86.
24. Kraulis, P. J. (1991) *J. Appl. Crystallogr.* **24,** 946–950.
25. Merritt, E. A. & Murphy, M. E. P. (1994) *Acta Crystallogr. D* **50,** 869–873.
26. Narayana, N., Cox, S., Xuong, N., Ten Eyck, L. F. & Taylor, S. S. (1997) *Structure (London)* **5,** 921–935.
27. Taylor, S. S., Radzio-Andzelm, E., Madhusudan, Cheng, X., Ten Eyck, L. F. & Narayana, N. (1999) *Pharmacol. Ther.* **82,** 133–141.
28. Tsigelny, I., Greenberg, J. P., Cox, S., Nichols, W. L., Taylor, S. S. & Ten Eyck, L. F. (1999) *Biopolymers* **50,** 513–524.
29. Knighton, D. R., Zheng, J. H., Ten Eyck, L. F., Ashford, V. A., Xuong, N. H., Taylor, S. S. & Sowadski, J. M. (1991) *Science* **253,** 414–420.
30. Hu, S. H., Parker, M. W., Lei, J. Y., Wilce, M. C., Benian, G. M. & Kemp, B. E. (1994) *Nature (London)* **369,** 581–584.
31. Kallunki, T., Su, B., Tsigelny, I., Sluss, H. K., Derijard, B., Moore, G., Davis, R. & Karin, M. (1994) *Genes Dev.* **8,** 2996–3007.
32. Kraut, J. (1988) *Science* **242,** 533–540.
33. Cannon, W. R., Singelton, S. F. & Benkovic, S. J. (1996) *Nat. Struct. Biol* **3,** 821–833.
34. Prowse, C. N. & Lew, J. (2000) *J. Biol. Chem.,* in press.
35. Kohen, A., Jonsson, T. & Klinman, J. P. (1997) *Biochemistry* **9,** 2603–2611.
36. Imoto, T., Ueda, T., Tamura, T., Isakari, Y., Abe, y., Inoue, M., Miki, T., Kawano, K. & Yamada, H. (1994) *Protein Eng.* **7,** 743–748.
37. Mine, S., Tate, S., Ueda, T., Kainosho, M. & Imoto, T. (1999) *J. Mol. Biol.* **286,** 1547–1565.